Electronic Supporting Information

Dinuclear Coordination Compounds based on a 5-Nitropicolinic Carboxylate Ligand with Single-Molecule Magnet Behaviour

Álvaro Raya-Barón,[a] Itziar Oyarzabal,[b] Francisco M. Arrabal-Campos,[a] José Manuel Seco,[b] Antonio Rodríguez-Diéguez*[,c] and Ignacio Fernández*[a,d]

[a] Department of Chemistry and Physics, University of Almería, Ctra. Sacramento s/n, 04120 Almería. [b] Department of Applied Chemistry, University of The Basque Country (UPV/EHU), 20018 San Sebastián, Spain. [c] Department of Inorganic Chemistry, University of Granada, 18071, Granada, Spain. [d] BITAL, Research Centre for Agricultural and Food Biotechnology, Ctra. Sacramento, s/n, E-04120, Almería, Spain. Corresponding Author: *E-mail: antonio5@ugr.es (A.R.-D.); ifernan@ual.es (I.F.).

CONTENTS

Figure S11. Temperature dependence of the $\chi_M T$ product for compound **3** in the presence of an external magnetic field H = 0.1 T (χ_M is the molar susceptibility per Dy^{3+} atom).

Figure S12. Temperature dependence of in-phase (top) and out-of-phase (middle) components of the ac susceptibility measured under 1000 Oe dc field for **3**. Inset: Arrhenius plots for the relaxation times. Bottom: Cole-Cole plots under 1000 Oe dc field.

Figure S13. Field dependence of the out-of-phase signal *vs* frequency at 4 K for **3**.

Modified Stokes-Einstein equation: Size and form factors.

Figure S14. ESI-MS spectrum for complex **2**.

Figure S15. Experimental and calculated ESI-MS spectra for the molecular ion of complex **2**.

Figure S16. ESI-MS spectrum for complex **3**.

Figure S17. Experimental and calculated ESI-MS spectra for the molecular ion of complex **3**.

Figure S18. FT-IR (KBr) spectrum of the yttrium complex **2**.

Figure S19. FT-IR (KBr) spectrum of the dysprosium complex **3**.

Table S1. Crystallographic details for structures of ligand **1**, and complexes of yttrium (**2**) and dysprosium (**3**).

Compound	**1**	**2**	**3**
Formula	$C_6H_6N_2O_5$	$C_{36}H_{30}N_{12}O_{30}Y_2$	$C_{36}H_{30}N_{12}O_{30}Dy_2$
M / g mol^{-1}	186.13	1288.54	1435.72
T (K)	100	100	100
λ/Å	0.71073	0.71073	0.71073
Cryst syst	Monoclinic	Monoclinic	Monoclinic
Space group	Cc	$P2_1/c$	$P2_1/c$
a / Å	5.112(3)	9.2140(4)	9.249(2)
b / Å	13.193(3)	29.2776(13)	29.630(3)
c / Å	22.059(3)	8.4568(4)	8.538(2)
α / °	90	90	90
β / °	92.561(5)	90.212(2)	90.503(4)
σ / °	90	90	90
V / Å^3	1486.2(9)	2281.32(18)	2339.8(8)
Z	8	2	2
ρ (g cm^{-3})	1.664	1.876	2.038
μ (mm^{-1})	0.148	2.651	3.286
Uniq. reflect.	4670	55957	14144
R (*int*)	0.049	0.034	0.087
GOF on F^2	1.126	1.351	1.143
R1 [I > 2σ(*I*)] [a]	0.099	0.036	0.126
wR2 [I > 2σ(*I*)] [a]	0.259	0.086	0.245

[a] $R(F) = \sum||F_o| - |F_c||/\sum|F_o|$; $wR(F^2) = [\sum w(F_o^2 - F_c^2)^2/\sum wF^4]^{1/2}$

Table S2.- Continuous Shape Measurements for the LnO_8 coordination environment. Low values indicate high proximity to the analyzed ideal geometry.

OP-8	1 D_{8h}	Octagon
HPY-8	2 C_{7v}	Heptagonal pyramid
HBPY-8	3 D_{6h}	Hexagonal bipyramid
CU-8	4 O_h	Cube
SAPR-8	5 D_{4d}	Square antiprism
TDD-8	6 D_{2d}	Triangular dodecahedron
JGBF-8	7 D_{2d}	Johnson gyrobifastigium J26
JETBPY-8	8 D_{3h}	Johnson elongated triangular bipyramid J14
JBTPR-8	9 C_{2v}	Biaugmented trigonal prism J50
BTPR-8	10 C_{2v}	Biaugmented trigonal prism
JSD-8	11 D_{2d}	Snub diphenoid J84
TT-8	12 T_d	Triakis tetrahedron
ETBPY-8	13 D_{3h}	Elongated trigonal bipyramid

	OP-8	**HPY-8**	**HBPY-8**	**CU-8**	**SAPR-8**	**TDD-8**	**JGBF-8**
Comp 2	29.660	23.380	14.856	9.990	1.183	2.019	13.811
Comp 3	29.675	23.063	14.742	9.985	1.284	2.092	13.757

	JETBPY-8	**JBTPR-8**	**BTPR-8**	**JSD-8**	**TT-8**	**ETBPY-8**
Comp 2	27.678	1.593	1.126	3.642	10.630	23.210
Comp 3	27.695	1.612	1.086	3.765	10.610	22.710

Table S3. Bond distances (Å) for compounds **1 – 3**.

1	**2**	**3**
C1A O2A 1.215(18)	Y1 O1B 2.2645(16)	Dy1 O1B 2.281(10)
C1A O1A 1.307(19)	Y1 O1W 2.2877(18)	Dy1 O1W 2.318(12)
C1A C2A 1.51(2)	Y1 O1A 2.3068(17)	Dy1 O1A 2.327(11)
C1B O2B 1.216(17)	Y1 O2W 2.3182(17)	Dy1 O2W 2.351(12)
C1B O1B 1.219(17)	Y1 O1C 2.3889(17)	Dy1 O1C 2.386(11)
C1B C2B 1.479(19)	Y1 O1C 2.4389(16)	Dy1 O1C 2.452(11)
C2A N1A 1.31(2)	Y1 N1C 2.517(2)	Dy1 N1C 2.525(14)
C2A C3A 1.42(2)	Y1 N1A 2.626(2)	Dy1 N1A 2.632(14)
C2B C3B 1.39(2)		
C2B N1B 1.42(2)		
C3A C4A 1.38(2)		
C3B C4B 1.32(2)		
C4A C5A 1.36(2)		
C4B C5B 1.35(2)		
C5A C6A 1.41(2)		
C5A N2A 1.45(2)		
C5B C6B 1.38(2)		
C5B N2B 1.49(2)		
C6A N1A 1.33(2)		
C6B N1B 1.39(2)		
N2A O3A 1.220(17)		
N2A O4A 1.227(17)		
N2B O3B 1.220(19)		
N2B O4B 1.312(18)		

Table S4. Bond angles (º) for compounds **1 - 3**

1	2	3
O2A C1A O1A 125.3(14)	O1B Y1 O1W 81.37(6)	O1B Dy1 O1W 81.1(4)
O2A C1A C2A 122.2(13)	O1B Y1 O1A 137.68(6)	O1B Dy1 O1A 137.3(4)
O1A C1A C2A 112.4(13)	O1W Y1 O1A 79.84(6)	O1W Dy1 O1A 79.5(4)
O2B C1B O1B 127.5(13)	O1B Y1 O2W 75.94(6)	O1B Dy1 O2W 75.8(4)
O2B C1B C2B 116.9(12)	O1W Y1 O2W 120.57(6)	O1W Dy1 O2W 121.1(5)
O1B C1B C2B 115.7(12)	O1A Y1 O2W 145.55(6)	O1A Dy1 O2W 146.0(4)
N1A C2A C3A 124.0(15)	O1B Y1 O1C 133.43(6)	O1B Dy1 O1C 134.0(4)
N1A C2A C1A 118.4(14)	O1W Y1 O1C 80.30(6)	O1W Dy1 O1C 81.7(4)
C3A C2A C1A 117.4(14)	O1A Y1 O1C 79.64(6)	O1A Dy1 O1C 79.8(4)
C3B C2B N1B 122.3(14)	O2W Y1 O1C 77.40(6)	O2W Dy1 O1C 77.3(4)
C3B C2B C1B 119.4(13)	O1B Y1 O1C 139.97(6)	O1B Dy1 O1C 139.8(4)
N1B C2B C1B 118.2(12)	O1W Y1 O1C 138.33(6)	O1W Dy1 O1C 138.7(4)
C4A C3A C2A 116.4(15)	O1A Y1 O1C 70.31(6)	O1A Dy1 O1C 70.9(4)
C4B C3B C2B 121.7(15)	O2W Y1 O1C 77.09(6)	O2W Dy1 O1C 76.9(4)
C5A C4A C3A 118.5(15)	O1C Y1 O1C 66.50(7)	O1C Dy1 O1C 65.5(5)
C3B C4B C5B 118.3(14)	O1B Y1 N1C 82.29(6)	O1B Dy1 N1C 83.2(4)
C4A C5A C6A 122.1(15)	O1W Y1 N1C 146.60(6)	O1W Dy1 N1C 146.2(5)
C4A C5A N2A 119.6(14)	O1A Y1 N1C 93.25(6)	O1A Dy1 N1C 92.4(5)
C6A C5A N2A 118.3(15)	O2W Y1 N1C 82.94(6)	O2W Dy1 N1C 83.2(5)
C4B C5B C6B 122.1(14)	O1C Y1 N1C 130.94(6)	O1C Dy1 N1C 129.4(4)
C4B C5B N2B 116.8(13)	O1C Y1 N1C 65.45(6)	O1C Dy1 N1C 64.8(4)
C6B C5B N2B 121.2(14)	O1B Y1 N1A 74.21(6)	O1B Dy1 N1A 74.5(4)
N1A C6A C5A 118.7(15)	O1W Y1 N1A 76.59(6)	O1W Dy1 N1A 76.0(4)
C5B C6B N1B 122.4(15)	O1A Y1 N1A 64.69(6)	O1A Dy1 N1A 64.0(4)
C2A N1A C6A 120.2(14)	O2W Y1 N1A 142.46(6)	O2W Dy1 N1A 142.5(4)
C6B N1B C2B 113.2(14)	O1C Y1 N1A 140.14(6)	O1C Dy1 N1A 140.1(4)
O3A N2A O4A 121.2(13)	O1C Y1 N1A 113.53(6)	O1C Dy1 N1A 113.6(4)
O3A N2A C5A 119.0(13)	N1C Y1 N1A 71.00(6)	N1C Dy1 N1A 71.0(5)

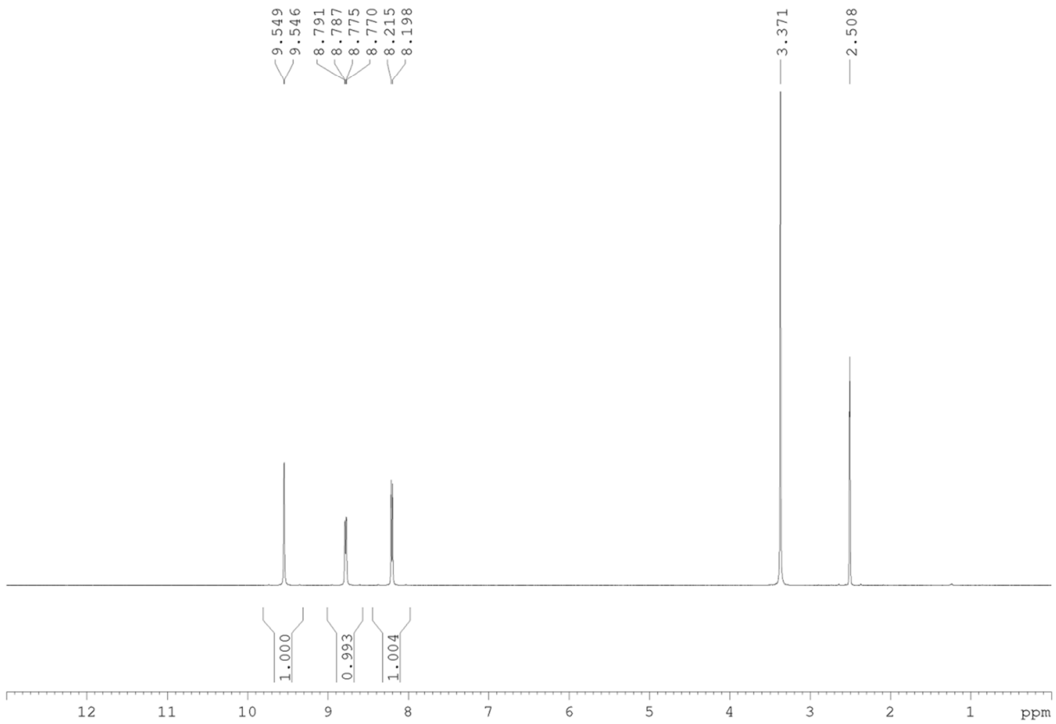

Figure S1. ^{1}H-NMR (500.13 MHz, DMSO-d_6) spectrum of complex **2**.

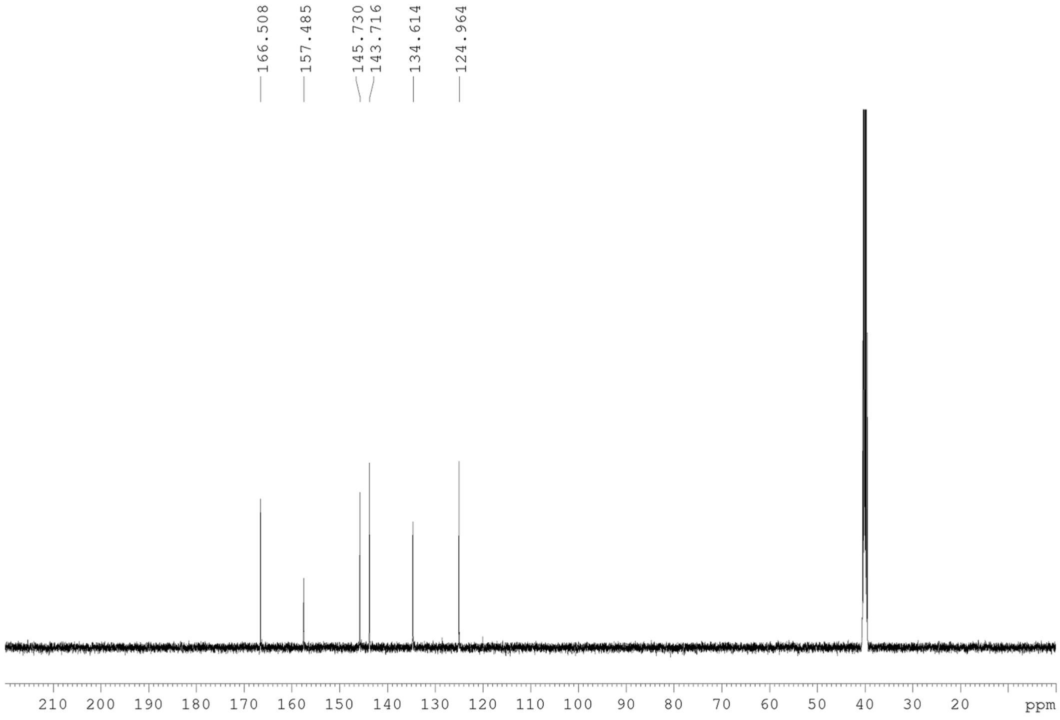

Figure S2. ^{13}C-NMR (125.76 MHz, DMSO-d_6) spectrum of complex **2**.

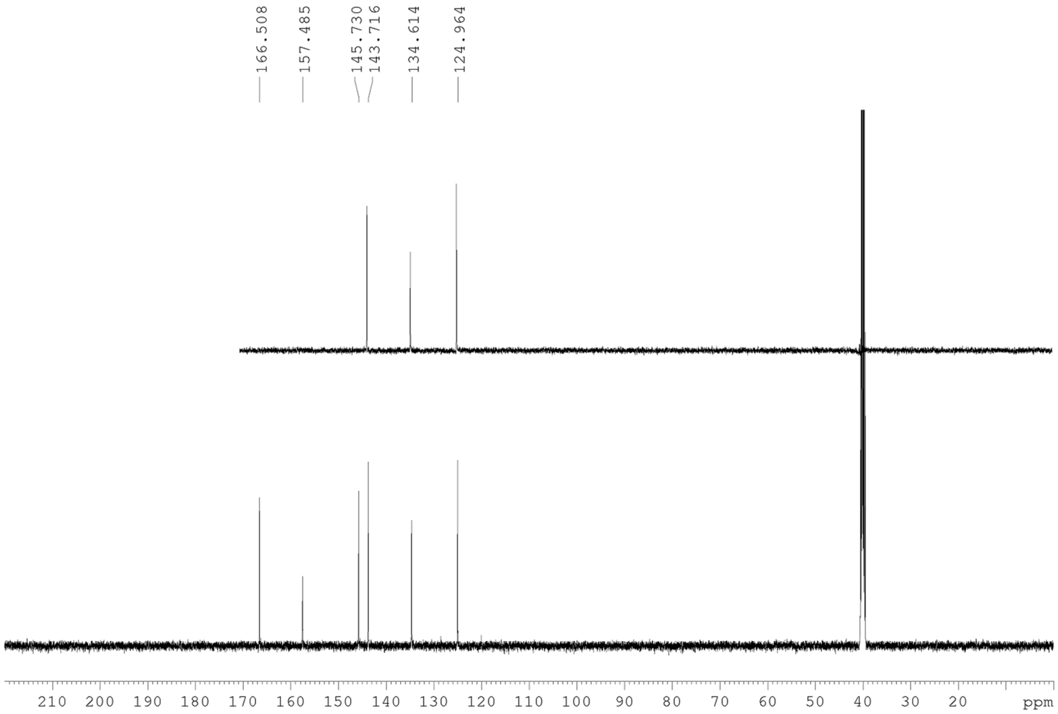

Figure S3. ^{13}C-NMR (125.76 MHz, DMSO-d_6) and DEPT-135 spectra of complex **2**.

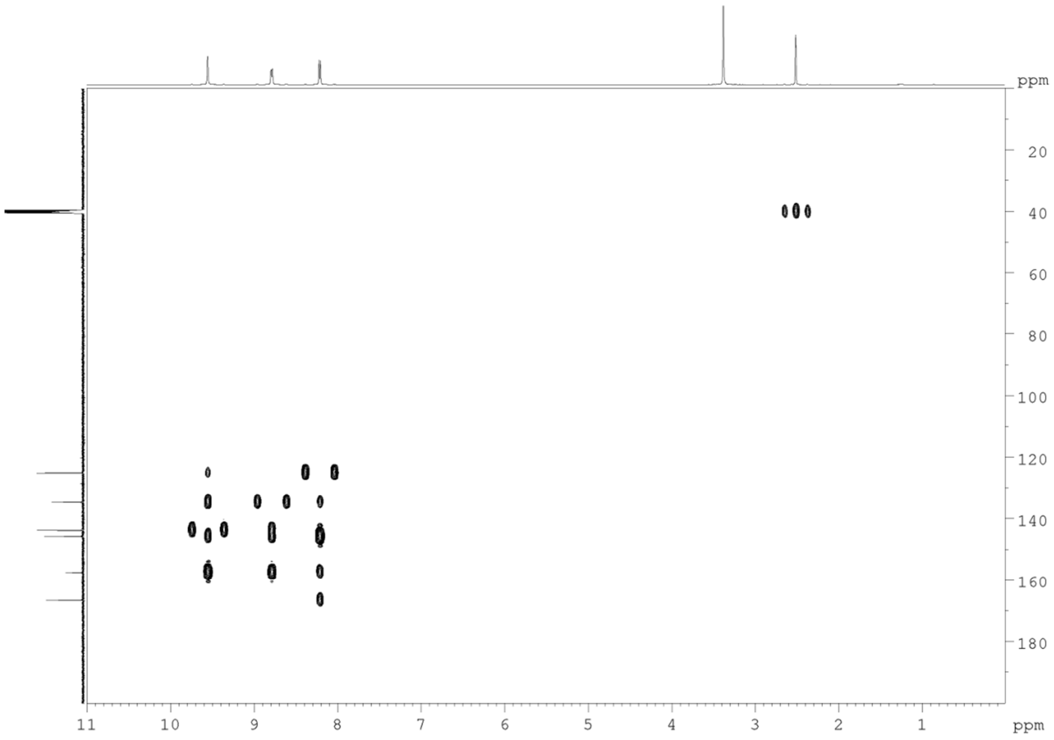

Figure S4. ^{1}H,^{13}C gHMBC spectrum of complex **2**.

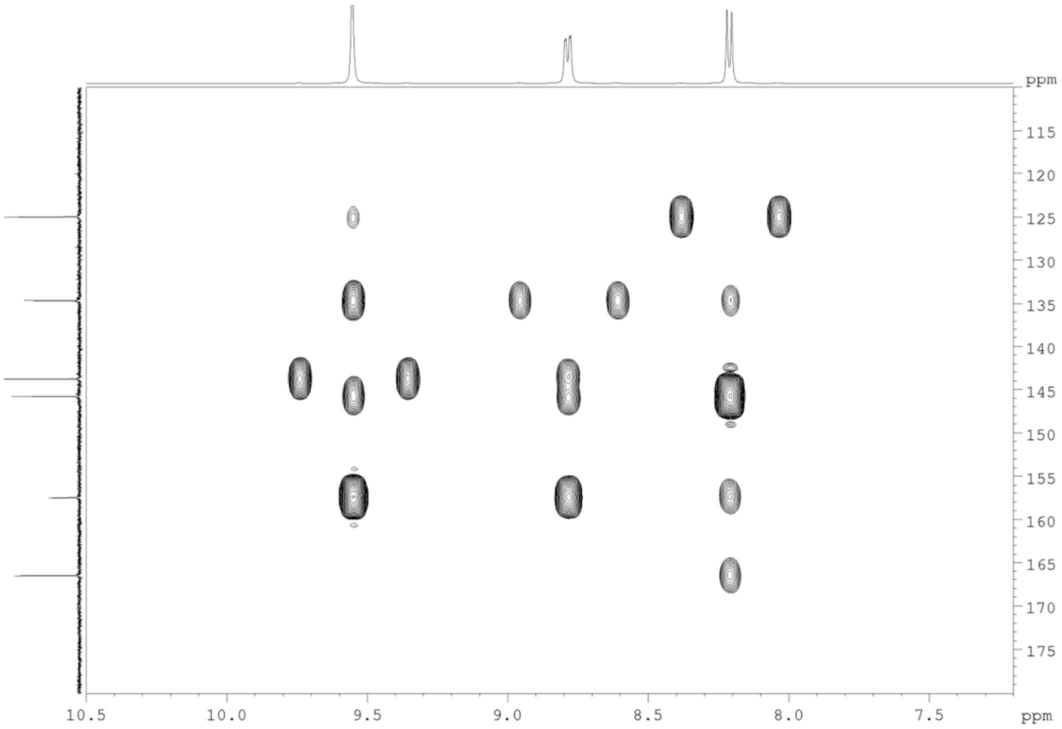

Figure S5. Expanded ^{1}H,^{13}C gHMBC spectrum of complex **2**.

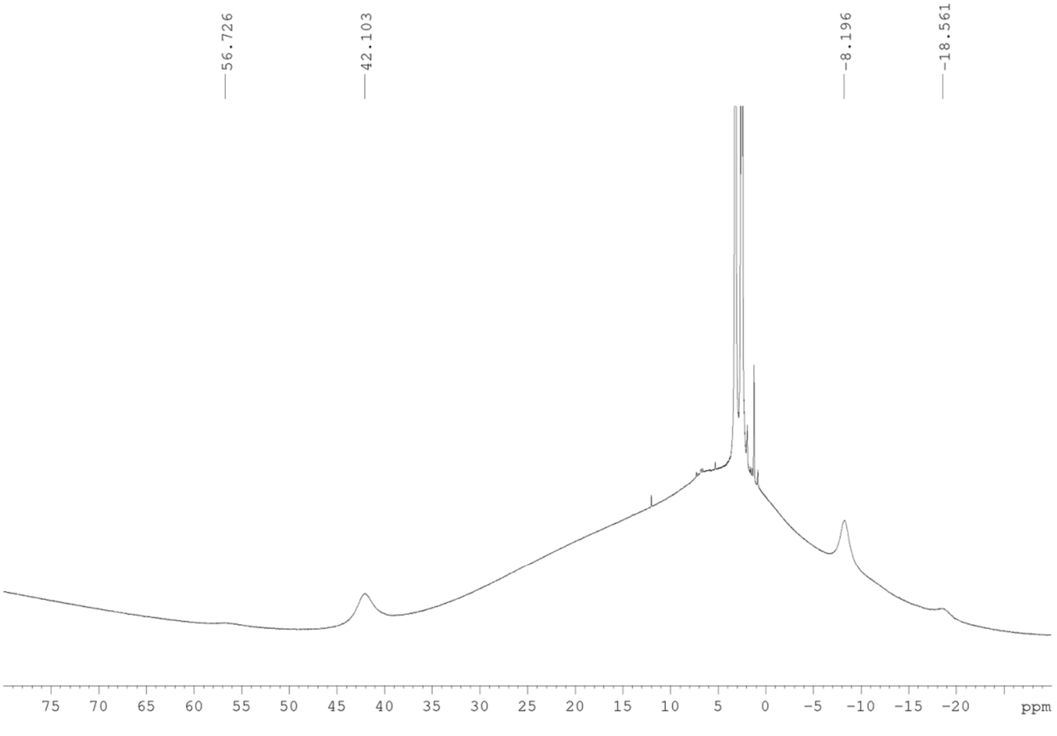

Figure S6. ^{1}H-NMR (500.13 MHz, DMSO-d_6) spectrum of complex **3**.

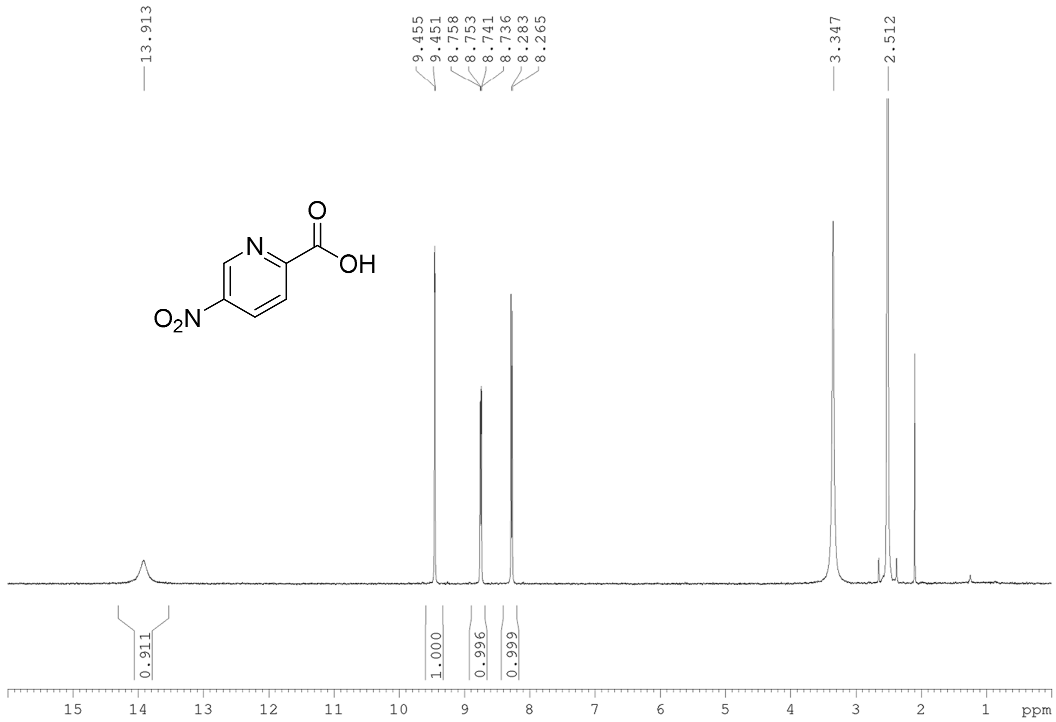

Figure S7. ^{1}H-NMR (500.13 MHz, DMSO-d_6) spectrum of 5-nitropicolinic acid.

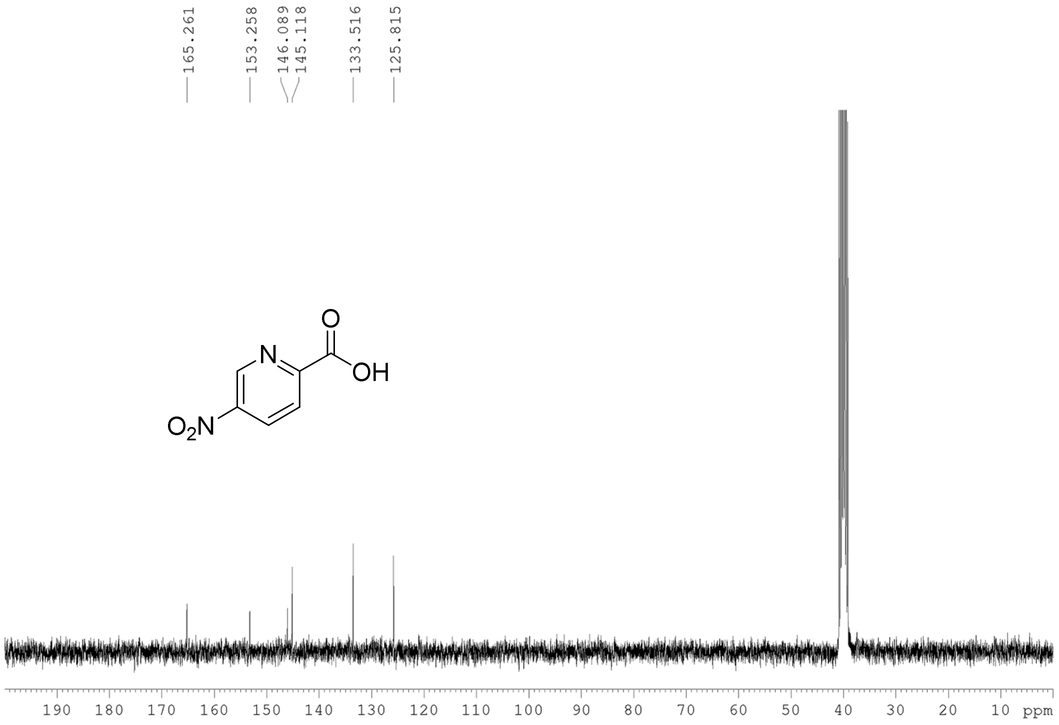

Figure S8. ^{13}C-NMR (125. 76 MHz, DMSO-d_6) spectrum of 5-nitropicolinic acid

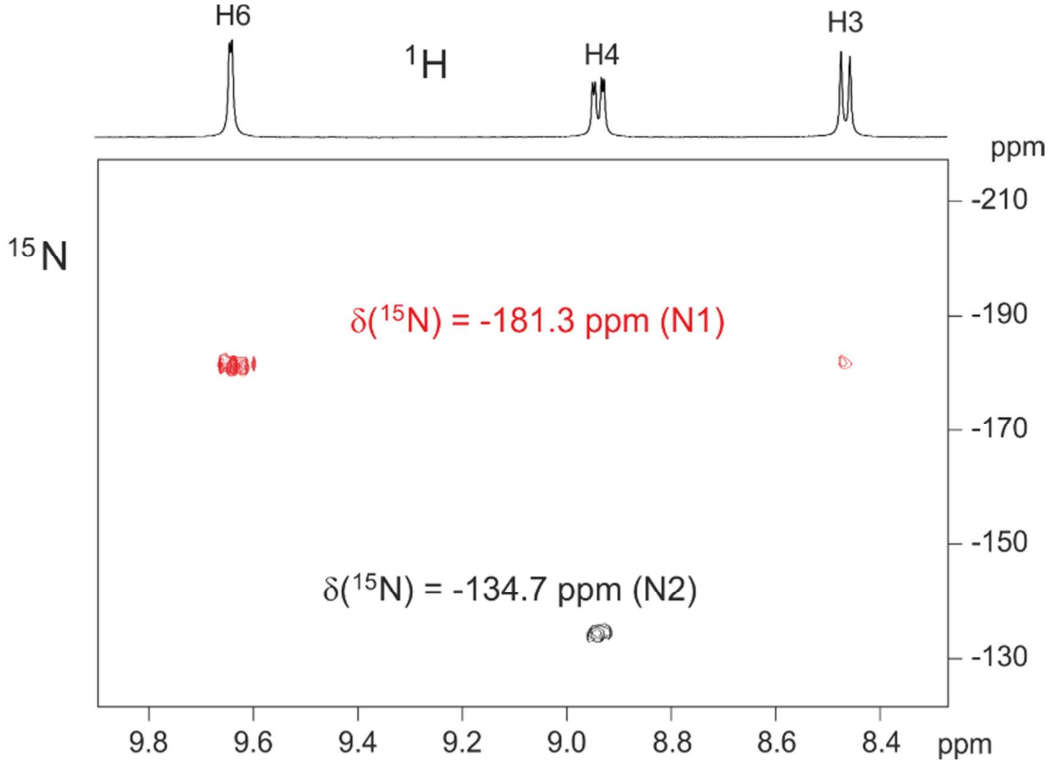

Figure S9. Section of the ^{1}H, ^{15}N gHMBC 2D NMR spectrum acquired in a 500 MHz spectrometer for a 180 mM sample of ligand **1** in DMSO-d_6 at 295 K. Complete data set was acquired in 4 h 33 min for 160-F1 series with a preparation delay optimized for a 7 Hz coupling constant and 80 of number of scans. The gradient ratio was calculated according to the γ values and set to 70:30:50.1.

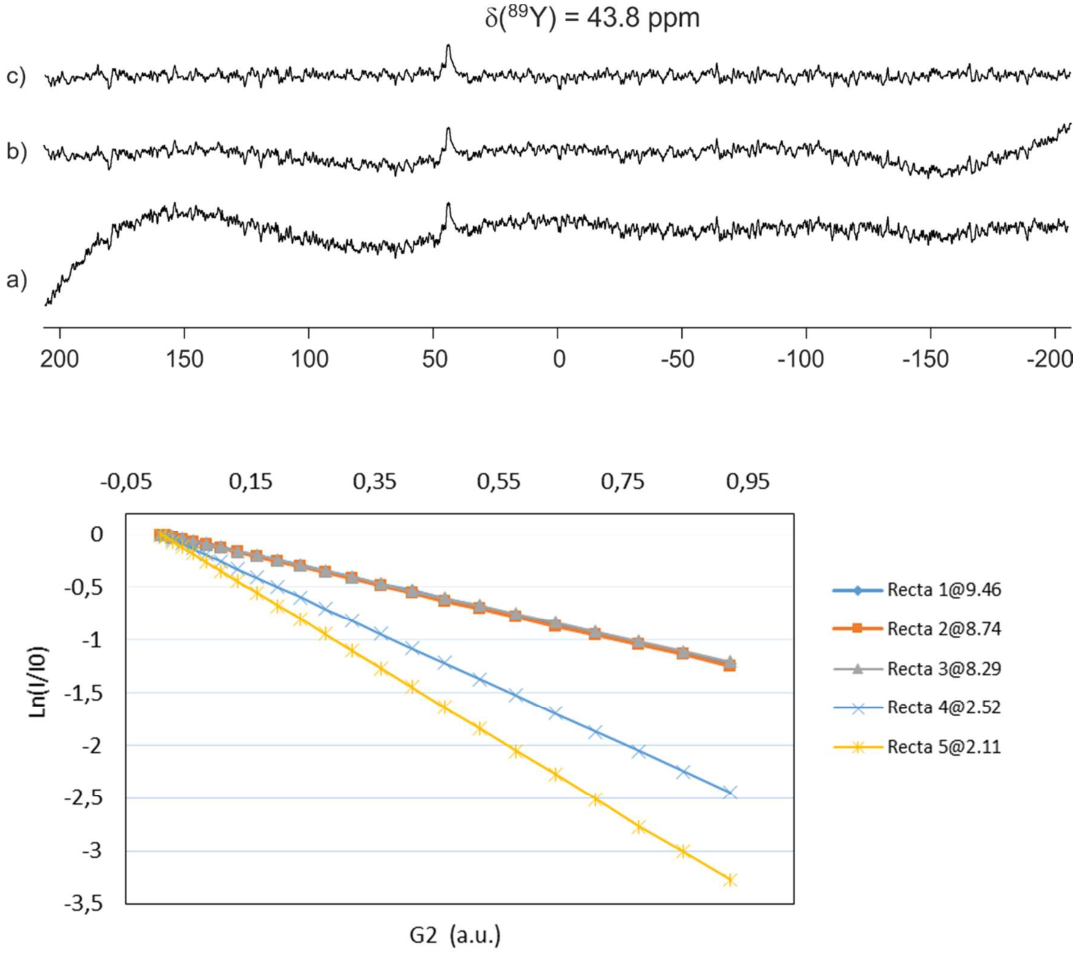

Figure S10. Top: a) 1D ^{89}Y NMR spectrum (24.5 MHz) for a saturated (20 mM) sample of complex **2** in DMSO-d_6 at 295 K (spectral window 12255 Hz). Complete data set was acquired in 61h with repetition delay of 20s, an inverse-gated sequence and a hard pulse of 30º (7.5 µs); b) 1D ^{89}Y NMR spectrum after elimination of the first 8 points of the FID before FT (with backwards linear prediction); c) 1D ^{89}Y NMR spectrum after elimination of the first 16 points of the FID before FT (with backwards linear prediction). Bottom: Stejskal-Tanner plots from ^{1}H PGSE diffusion experiments in DMSO-d_6 at room temperature, using the stimulated echo sequence, of ligand **1** at 60 mM. The solid lines represent linear least-squares fits to the experimental data. Yellow and blue lines correspond to the attenuation of H_2O and DMSO, respectively.

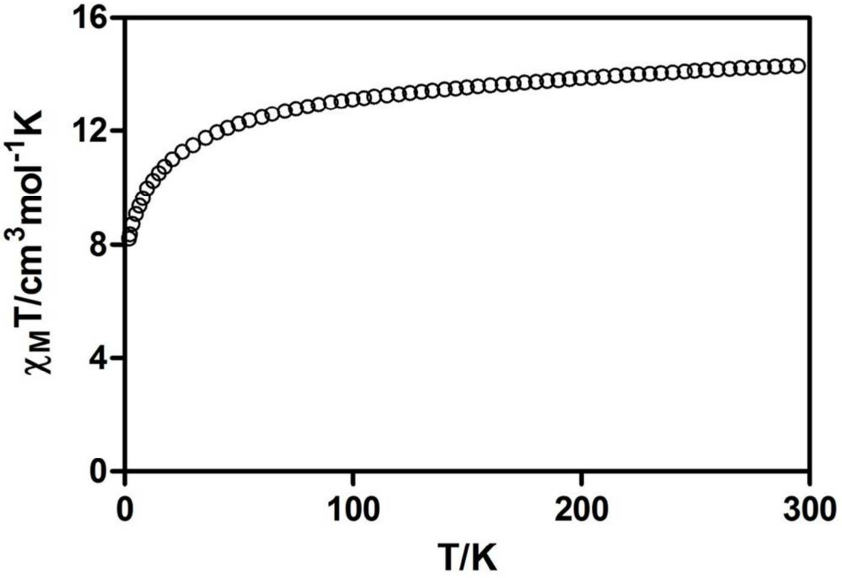

Figure S11. Temperature dependence of the $\chi_M T$ product for compound **3** in the presence of an external magnetic field H = 0.1 T (χ_M is the molar susceptibility per Dy^{3+} atom).

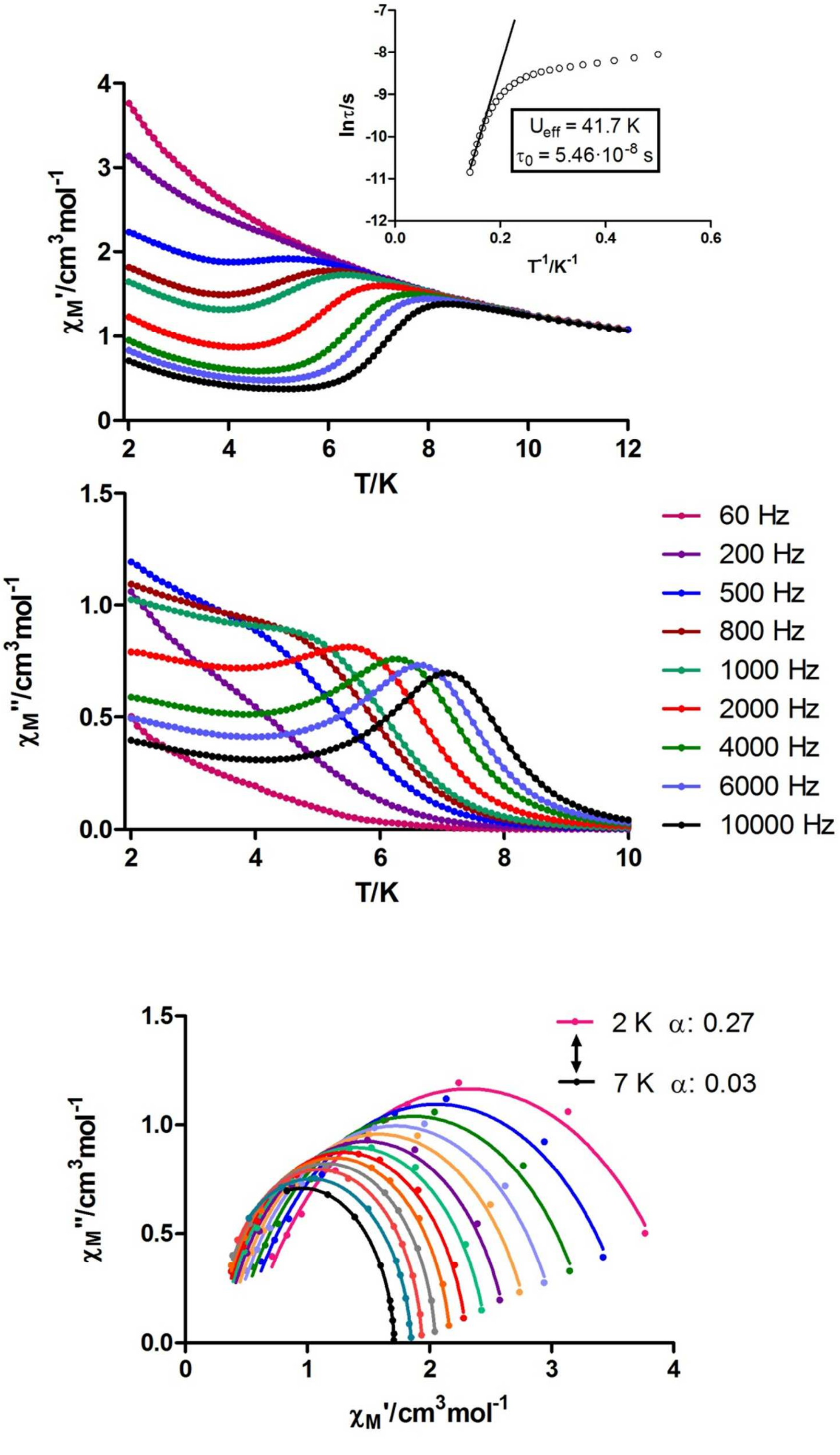

Figure S12. Temperature dependence of in-phase (top) and out-of-phase (middle) components of the ac susceptibility measured under 1000 Oe dc field for **3**. Inset: Arrhenius plots for the relaxation times. Bottom: Cole-Cole plots under 1000 Oe dc field.

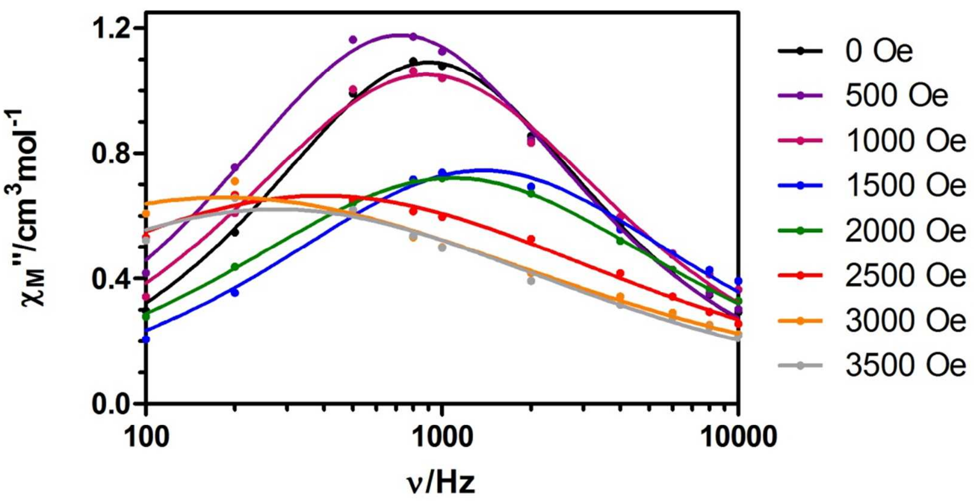

Figure S13. Field dependence of the out-of-phase signal *vs* frequency at 4 K for **3**.

Modified Stokes-Einstein equation: Size[1] and form[2] factors. The equations that should be considered are summarized below.

$$D = \frac{kT}{c(r_{sl}, r_h) f_s(a,b) \eta r_h}$$

$$c(r_{sl}, r_h) = \frac{6}{1 + 0.695 \left(\frac{r_{sl}}{r_H}\right)^{2.234}}$$

$$p = \frac{height}{width} = \frac{a}{b} = \frac{L}{\phi}$$

$$\gamma = 0.312 + \frac{0.565}{p} + \frac{0.1}{p^2}$$

$$f_s = \frac{\left(\frac{2p^2}{3}\right)^{\frac{1}{3}}}{\ln(p) + \gamma}$$

$$Volume_{sphere} = Volume_{cylinder}$$

$$\frac{\pi \phi_{sphere}^3}{6} = \frac{\pi \phi_{cylinder}^2}{4} L$$

$$\phi_{cylinder} = \phi_{sphere} \sqrt[3]{\frac{22}{57}}$$

In order to calculate these factors we have executed a recursive algorithm. The radius (r_{sl}) of DMSO employed was set to 1.56 Å. The c coefficient obtained was 5.833 and the factor shape $f_s(a,b)$ deduced was 1.03. The semiaxis of the cylinder were 7.77 and 4.73 Å for a and b, respectively. Both factors gave us a hydrodynamic radius for complex **2** equal to 6.5 Å.

The programmed code is:

```
%%Chen and form calculation
k = 1.38065*10^(-23); %Boltzmann constant
T = 294; % Temperature (K)
h = 0.002077; %Viscosity value (k/m2)
DDMSO = 6.655*10^(-10);  % Diffusion coefficient of DMSO
rHDMSO = k*T/(6*pi*h*DDMSO); % rH of DMSO
D2 = 1.593*10^(-10); % Diffusion coefficient of 2
rH2 = 2*k*T/(6*pi*h*D2); % rh of 2
a = 19;
b =11;
p = a/b; % Relation among height and width
gamma = 0.312+0.565/p+0.1/p^2;
fs = (2*p^2/3)^(1/3)/(log(p)+gamma); % Cylinder approximation;
N = 20; % N iteration
% Recursive algorithm
for i = 1:N
    C(i) = 6/(1+0.695*(rHDMSO/rH2)^2.234)
    rH2 = k*T/(C(i)*fs*pi*h*D2);
end
```

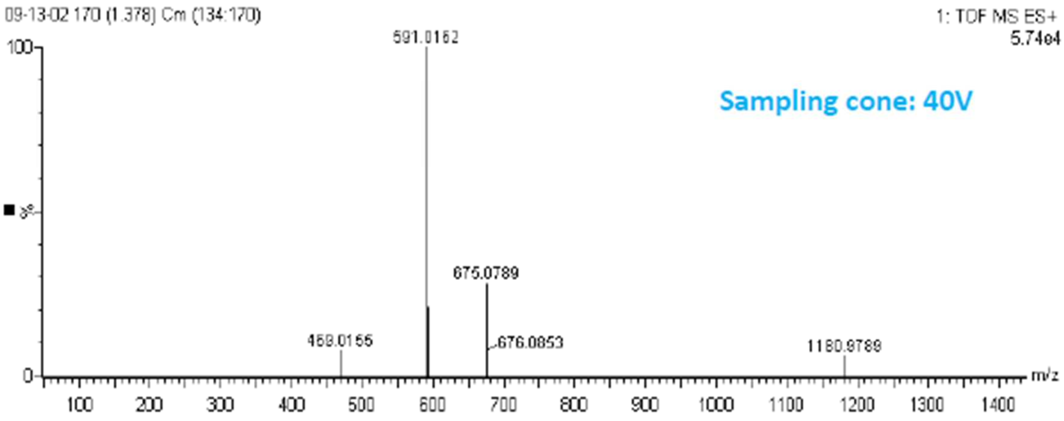

Figure S14. ESI-MS spectrum for complex **2**.

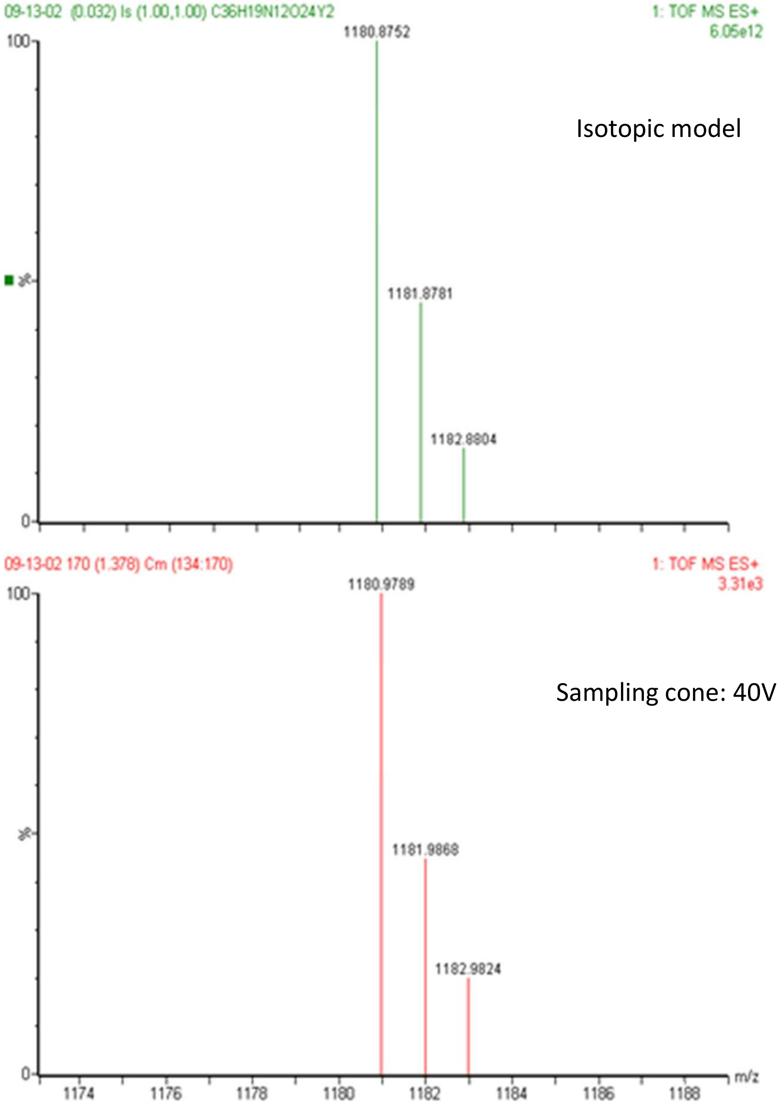

Figure S15. Experimental and calculated ESI-MS spectra for the molecular ion of complex **2**.

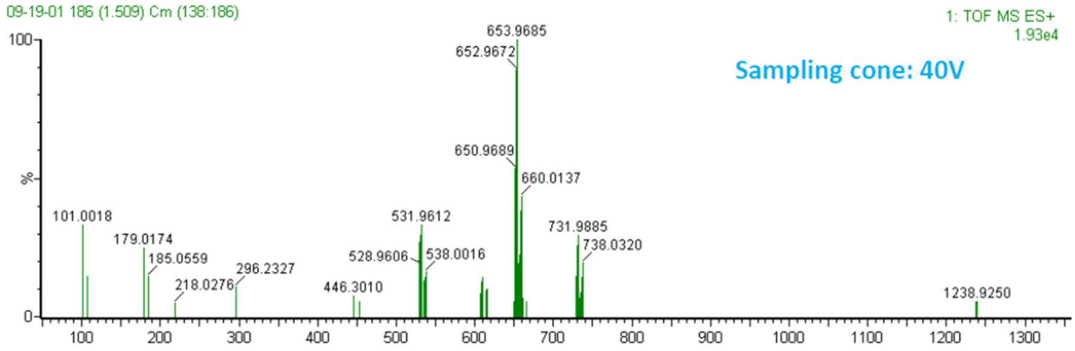

Figure S16. ESI-MS spectrum for complex **3**.

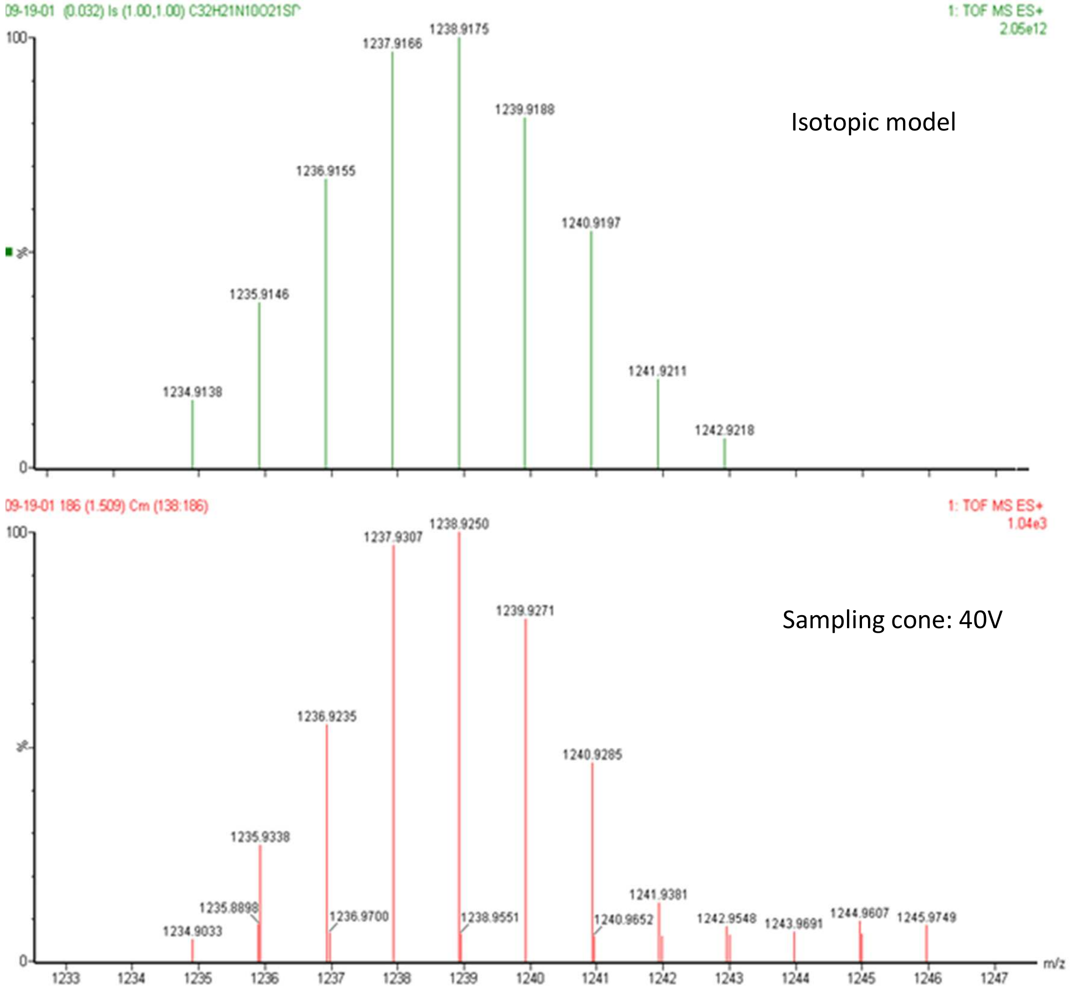

Figure S17. Experimental and calculated ESI-MS spectra for the molecular ion of complex **3**.

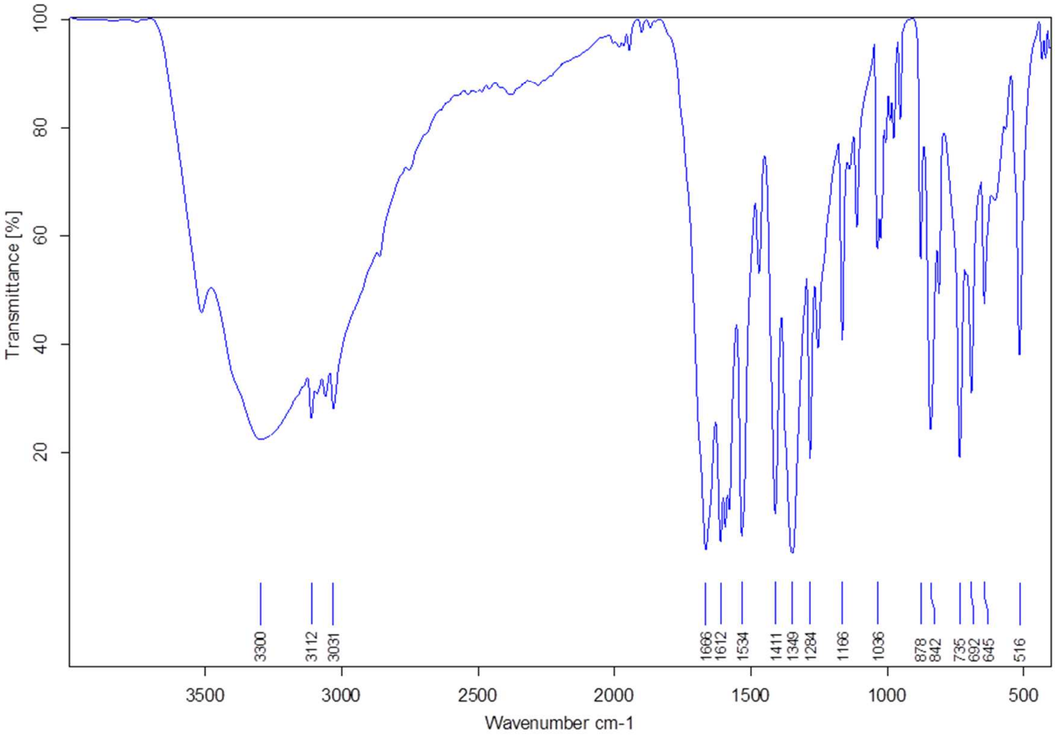

Figure S18. IR (KBr) spectrum of the yttrium complex **2**.

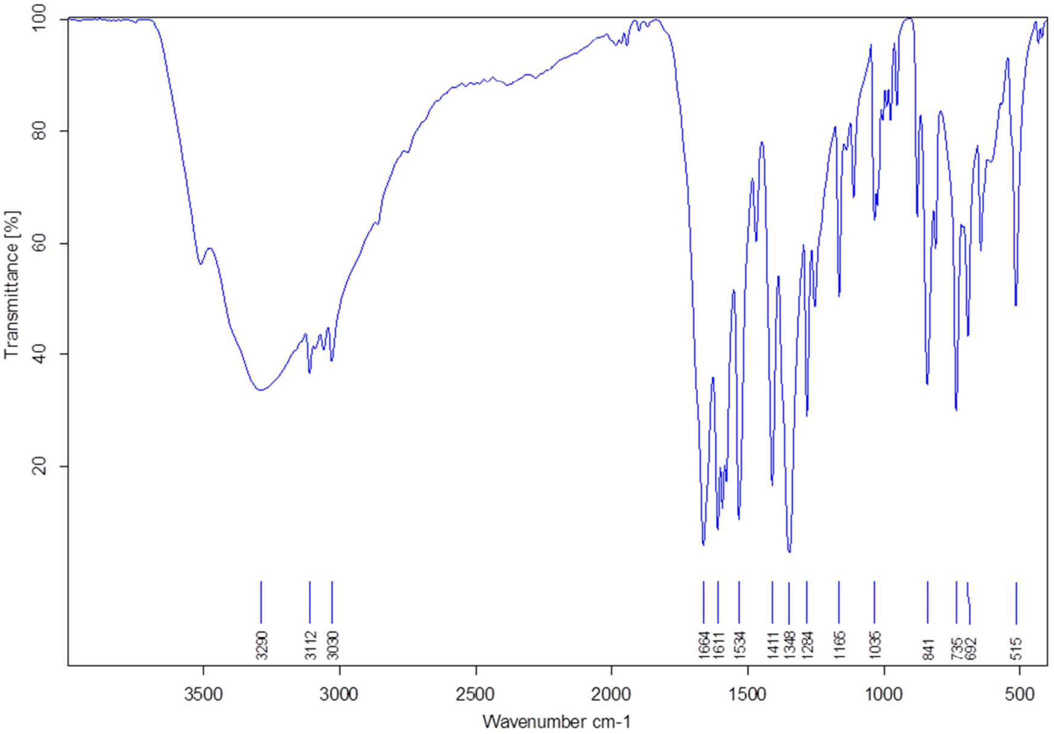

Figure S19. IR (KBr) spectrum of the dysprosium complex **3**.

As can be seen in both spectra, after coordination to lanthanide ions the bands corresponding to the C=O stretching vibrations (at around 1700 and 1730 cm^{-1} for 5-nitropicolinic acid, see http://webbook.nist.gov/cgi/inchi?ID=C30651242&Mask=80) move to lower wavenumbers (below 1664-1666 cm^{-1}), as expected. The assignment of the bands found in the 1666-1534 cm^{-1} range and the identification of their relation with the different coordination modes of the carboxylate groups is not easy to do due to the diverse origin of the bands that appear in this region (C=O stretching, N-O asymmetric stretching of the nitro group and aromatic C=C stretching). In both spectra, the most intense band at 1348-1349 cm^{-1} comes from the symmetric N-O stretching of the nitro group.

References

---

[1] a) Spernol, A. and Wirtz, K. *Z. Naturforsch., A: Astrophys., Phys. Phys. Chem.*, **1953**, *8*, 522–532; b) Chen, H.C. and Chen, S.H. *J. Phys. Chem.,* **1984**, *88*, 5118–5121; c) Macchioni, A.; Ciancaleoni, G.; Zuccaccia, C. and Zuccaccia, D. *Supramolecular Chemistry: From Molecules to Nanomaterials*, John Wiley Sons Ltd, vol. 2, ch. 4, 2012.

[2] Tirado, M.M.; Lopez Martinez, C. and Garcia de la Torre, J.J. *Chem. Phys.*, **1984**, *81*, 2047–2052.